Model-Based Sensorimotor Integration for Multi-Joint Control: Development of a Virtual Arm Model

4 authors, including:

Some of the authors of this publication are also working on these related projects:

Synergy-based NMES for stroke rehabilitation View project

NuStim View project

Model-Based Sensorimotor Integration for Multi-Joint Control: Development of a Virtual Arm Model

D. Song,[1] N. Lan,[2] G. E. Loeb,[1] and J. Gordon[2]

[1]Department of Biomedical Engineering, University of Southern California, Los Angeles, CA 90089, USA; and [2]Department of Biokinesiology and Physical Therapy, University of Southern California, Los Angeles, CA 90089, USA

Abstract—An integrated, sensorimotor virtual arm (VA) model has been developed and validated for simulation studies of control of human arm movements. Realistic anatomical features of shoulder, elbow and forearm joints were captured with a graphic modeling environment, SIMM. The model included 15 musculotendon elements acting at the shoulder, elbow and forearm. Muscle actions on joints were evaluated by SIMM generated moment arms that were matched to experimentally measured profiles. The Virtual Muscle™ (VM) model contained appropriate admixture of slow and fast twitch fibers with realistic physiological properties for force production. A realistic spindle model was embedded in each VM with inputs of fascicle length, gamma static (γ_{stat}) and dynamic (γ_{dyn}) controls and outputs of primary (I_a) and secondary (II) afferents. A piecewise linear model of Golgi Tendon Organ (GTO) represented the ensemble sampling (I_b) of the total muscle force at the tendon. All model components were integrated into a Simulink block using a special software tool. The complete VA model was validated with open-loop simulation at discrete hand positions within the full range of α and γ drives to extrafusal and intrafusal muscle fibers. The model behaviors were consistent with a wide variety of physiological phenomena. Spindle afferents were effectively modulated by fusimotor drives and hand positions of the arm. These simulations validated the VA model as a computational tool for studying arm movement control. The VA model is available to researchers at website http://pt.usc.edu/cel.

Keywords—Computational models, Joints, Muscles, Spindles, GTO, Sensorimotor control, Simulation, Matlab and Simulink.

INTRODUCTION

Sensorimotor dynamics and musculoskeletal biomechanics present inevitable constraints on motor control strategies that are evolved in the brain. The effects of these peripheral constraints on central control could not be evaluated with models in many previous studies, which have generally been limited to the particular subsets of the neuro-musculoskeletal system. These previous models were developed such that they were most relevant to the experimental phenomena under study with simplifying assumptions in order to fit the experimental results. Recently, it was recognized that systems models that were based on the neurophysiology and biomechanics of the sensorimotor system could expand the utility of modeling approach in parallel with experimental investigation.[2,30] Hierarchical models of the neuron-musculoskeletal system were employed to investigate control strategies of arm postures and reaching movements,[27,29,36] as well as neural control of locomotion.[51] A simulation study with a systems α-γ model suggested a plausible role for proprioceptive reflexes in controlling joint equilibrium position by way of γ static fusimotor command.[30] Such a systems model may also help explain the behaviors observed in deafferented patients,[19,21] and provide insights into the roles of proprioceptive afferents in neural control of movement that was revealed with muscle percussion.[9,12] Realistic models of neuro-sensorimotor system could also provide a computational tool for neuroscientists to understand plausible neural strategies that are usually inferred indirectly from behavioral, psychophysical and electrophysiological data.

There have been many recent advances in the sophistication and completeness of individual model components,[10,35,37,38,52] and in the tools necessary to embody specific model structures in the computational environment in which the models run.[3,15,24] All of these now make it feasible to develop a realistic multi-joint, multi-muscle virtual arm (VA) model for computational studies of human motor control and learning. The VA model described here has shoulder, elbow and forearm degrees of freedom (DOF) with 15 muscles. The spindle and GTO models are embedded in each muscle to provide afferent information about the state of muscle contraction. The VA model is able to
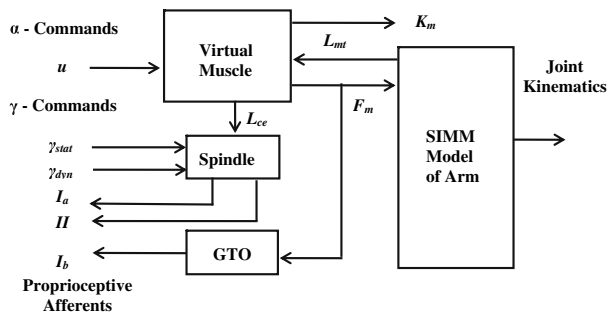
FIGURE 1. Diagram for the sensorimotor systems model integration. The Virtual Muscle receives α-command (*u*) and produces force outputs to drive SIMM musculoskeletal model for joint kinematics. The joint dynamics in turn passes the changes in musculotendon length (L_{mt}) back to the Virtual Muscle models. GTO model receives muscle force output from Virtual Muscle blocks and produce I_b afferent firings. Muscle Spindle model is driven by dynamics, static γ-commands (γ$_{stat}$, γ$_{dyn}$) and muscle fascicle lengths (L_{ce}) from Virtual Muscle blocks, and outputs primary (I_a) and secondary (II) firings.

calculate muscle stiffness analytically from the virtual muscle model. The VA model integrates individual component models of skeleton, virtual muscle, spindle, and GTO into a systems model (Fig. 1). Each of the component models is validated in isolated physiological conditions, and the parameters of the component models are determined in their prior validation in the development. Only those that are related to operation in the integrated system need to be adjusted, e.g., muscle length–tension property. The validation of the integrated model is, thus, focused on whether the gross behavior of system inputs and outputs is consistent to sensorimotor physiology, when operating condition and muscle activation, rather than model parameters, are changed. The VA model is validated in this study with open-loop dynamic simulations at different hand positions in space and with the full range of α and γ inputs to the muscles and spindles. This model could be further integrated with neural control elements of the central nervous system (CNS) for simulation studies in motor control and learning. It could also be modified to simulate abnormal behaviors of the human motor system under various pathological conditions, e.g., deafferentation, stroke and spinal cord injury. Preliminary results have been reported elsewhere.[32,46]

MATERIALS AND METHODS

The VA model was constructed from a set of component models, i.e., a musculoskeletal model, the virtual muscle (VM), the spindle model, and a GTO model. A systems model of the complete VA is shown in Fig. 1, in which these model components are integrated to give rise to the outputs of joint kinematics

and proprioceptive afferents under descending muscle (α) and spindle (γ) inputs. In the following sections, the component models and their integration are described.

Musculoskeletal Model

Skeletal Structure

The musculoskeletal arm model was developed in a graphical modeling environment, SIMM (version 3.2), which is a widely used modeling software.[15] Part of the musculoskeletal structure of shoulder complex was based on the model developed by Holzbaur *et al.*[24] The rest of the bony structure of the VA was based on an elbow model in SIMM.[28,31] Figure 2a shows the planar view of the right arm in SIMM. The skeletal system consists of the thorax complex, including the thorax, the sternum, the clavicle and the scapula. The arm contains the humerus, the radius, the ulna and the wrist/hand bones. Figure 2b shows the 15 muscles across the shoulder, elbow and forearm joints: deltoid anterior (DA), deltoid posterior (DP), the clavicular portion of pectoralis major (PC), supraspinatus (SS), infraspinatus (IS), biceps long head (Blh), biceps short head (Bsh), triceps long head (Tlh), triceps lateral head (Tlt), triceps medial head (Tmd), brachialis (BS), brachioradialis (BR), pronator teres (PT), pronator quadratus (PQ), and supinator (SP). The thorax complex stands as a ground for the arm and as a reference of the clavicle and scapular bones, which provide the attaching sites for shoulder muscles. The model does not yet include muscles operating the wrist and finger joints, so these joints are fixed in the posture illustrated and the segments contribute only to the mass and inertial properties of the forearm, a common constraint of many experimental paradigms for studying reaching movements.[1,21,23]

Joint Kinematics

The coordinate systems for each segment as shown in Fig. 2a are defined according to the convention recommended by the International Society of Biomechanics.[50] The local coordinate system of the thorax coincides with the world coordinate system. The positions of clavicle and scapula relative to thorax are fixed at 30° based on the shoulder rhythms when humerus is elevated (abducted) at 90° in the frontal plane.[24] The articulation between the scapula and humerus (glenohumerus or GH joint) is modeled as a ball-and-socket joint, with the center of the rotation located at the origin of the humerus local coordinate system. In the present model, the motion of the GH joint is constrained to the horizontal flexion/extension, because of available measurements of shoulder muscle moment arm are obtained in this plane, and the majority of studies in movement control are
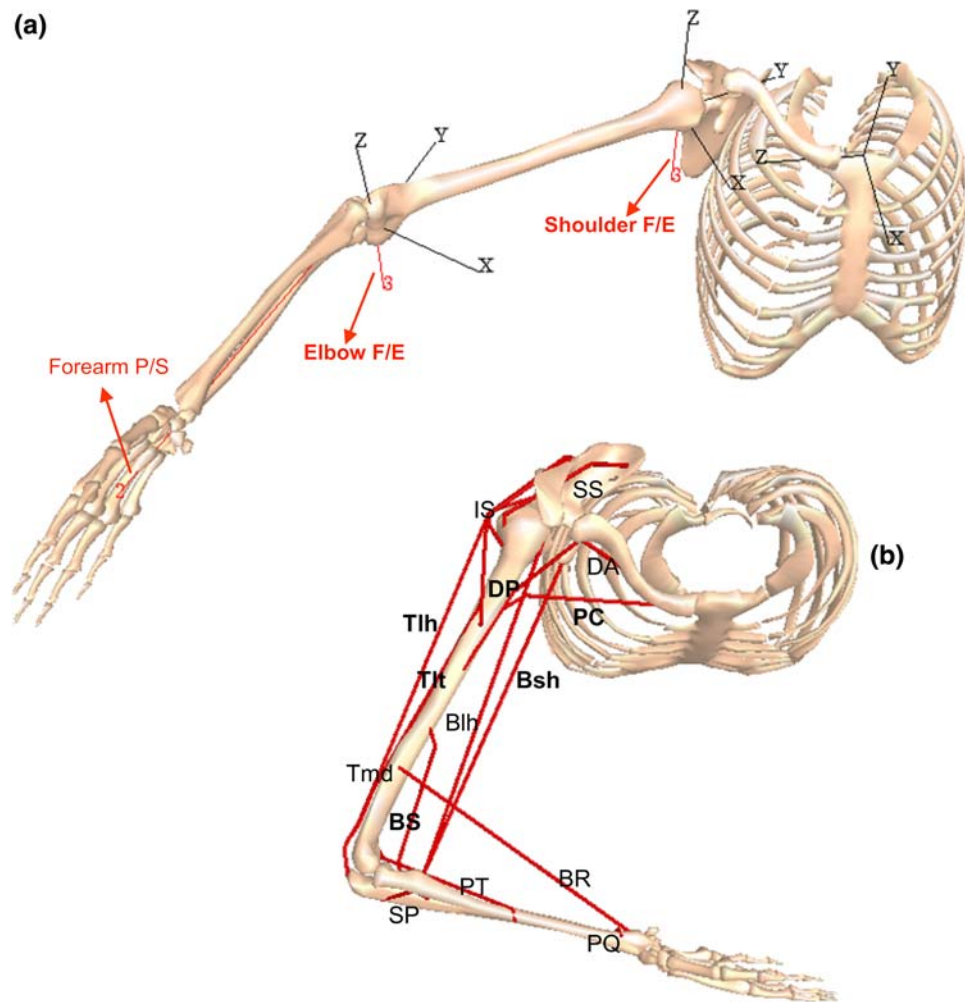
FIGURE 2. The VA musculo-skeletal model in SIMM. (a) The planar view of right arm skeletal model demonstrating the segments (ribs, sternum, clavicle, scapular, humerus, radius, ulna, and bones of the wrist and hand), the joint coordinate systems, the degrees of freedom (DOF), shoulder flexion/extension (F/E), elbow F/E and forearm pronation/supination (P/S). (b) The origin, insertion points and paths of the 15 major muscle elements across the three joints (shoulder, elbow, and forearm) of skeletal model. The 15 muscle elements include: deltoid anterior (DA), deltoid posterior (DP), clavicle portion of pectoralis major (PC), supraspinatus (SS), infraspinatus (IS), biceps long (Blh), biceps short (Bsh), triceps long (Tlh), triceps lateral (Tlt), triceps medial (Tmd), brachialis (BS), brachioradialis (BR), pronator teres (PT), pronator quadratus (PQ), and supinator (SP). The thorax functions as a ground and was included as the reference of the clavicle and scapular, which provided the attachment sites for shoulder muscles. The 2 DOF and 6 muscles used in later simulation are bold labeled in (a) and (b).

constrained to planar motion at shoulder level. However, this constraint can be easily removed for more general purpose of motion simulation. The elbow (or humeroulnar) joint is modeled as a hinge joint with the rotation axis passing between the center of the trochlear sulcus of the ulna and the center of the capitulum of the humerus with a carrying angle at about 5°. The forearm rotates about an axis that passes through the center of the proximal radius and the center of the styloid process of the distal ulna. The range of elbow flexion is from 0° (fully extended) to 130° (fully flexed), and forearm rotation from −10° (fully supinated) to 180° (fully pronated). The neutral position of the forearm (0° of pronation) is defined to keep the hand in

the elevation plane as the arm stays in the horizontal plane at shoulder level.

Muscle Origin/Insertion Points and Musculotendon Paths

Muscle insertion and origin points (I/O points) were defined with a single point contact to bone surface. Muscle I/O points were initially chosen according to their anatomical landmarks; via-points in the muscolotendon path and wrapping surfaces attached to the underlying bone segments were defined to represent the anatomical constraints at joints and in musculotendon paths over the full range of joint motion. I/O, via points

and wrapping surfaces were adjusted as necessary to match experimentally measured values of moment arms from the literature.[22,40] Measurements of shoulder moment arms in cadaver specimens are available only for horizontal flexion.[26] Because experimental moment arms in elbow and forearm muscles were obtained with the shoulder joint at its neutral position (i.e., 0° of elevation), SIMM generated moment arms of these muscles were fitted to experimental data in the similar neutral position of shoulder joint, where the humerus is in parallel with the Y axis of the thorax. Muscle I/O points in local coordinates are listed in Table 1.

Segmental and Inertial Parameters

Inertial parameters used in the VA model are listed in Table 2. The size of bones was measured from SIMM, and was close to the cadaver measurements in.[48] Thus, the segment masses and inertias measured by[48] was used in this model. The center of mass of each segment was estimated as a percentage of the segmental length from the proximal end of the bones.[44] Since forearm mass and inertia were measured as properties of lumped radius and ulna in,[48] their values were evenly distributed to radius and ulna segments in the model.[34]

Virtual Muscle Model Parameters

Virtual Muscle Parameters

The virtual muscle (VM) model implemented in this system is a modified version of the original VM model of Cheng *et al.*[10] For details of modification, audience is referred to an online appendix provided at website http://pt.usc.edu/cel.

TABLE 1. Muscle origin (O) and insertion (I) points.

Muscle	Abbreviation	Bones (O—origin; I—insertion)	x (cm)	y (cm)	z (cm)
Shoulder					
Deltoid					
Anterior	DA	Clavicle (O)	−0.95	0.82	6.75
		Humerus (I)	0.60	−11.38	0.68
Posterior	DP	Scapula (O)	−5.57	0.12	−2.51
		Humerus (I)	0.21	−7.60	1.05
Supraspinatus	SS	Scapula (O)	−5.59	−0.03	−8.10
		Humerus (I)	−1.54	−0.11	1.56
Infraspinatus	IS	Scapula (O)	−7.79	−3.59	−6.62
		Humerus (I)	−1.13	−1.33	1.31
Pectoralis major					
Clavicular	PC	Clavicle (O)	0.80	−0.22	3.29
		Humerus (I)	1.22	−5.83	0.48
Elbow					
Biceps					
Long	Blh	Scapula (O)	−3.12	−2.35	−1.31
		Radius (I)	0.96	−3.68	0.38
Short	Bsh	Scapula (O)	1.10	−3.92	−2.79
		Radius (I)	1.00	−3.68	0.37
Triceps					
Lateral	Tlt	Humerus (O)	−0.44	−5.95	0.70
		Ulna (I)	−1.89	1.27	0.02
Long	Tlh	Scapula (O)	−4.86	−4.68	−1.71
		Ulna (I)	−1.89	1.27	0.02
Medial	Tmd	Humerus (O)	−0.84	−13.70	−0.91
		Ulna (I)	−1.89	1.27	0.02
Brachialis	BS	Humerus (O)	0.40	−16.96	0.04
		Ulna (I)	−0.85	−3.03	0.46
Brachioradialis	BR	Humerus (O)	−0.41	−20.88	0.07
		Radius (I)	0.49	−20.86	2.63
Major forearm					
Pronator teres	PT	Humerus (O)	0.99	−28.17	−2.81
		Radius (I)	−0.54	−11.44	2.92
Pronator quadratus	PQ	Ulna (O)	−2.27	−21.17	1.61
		Radius (I)	0.14	−20.23	3.41
Supinator	SP	Ulna (O)	−2.96	−1.38	−0.37
		Radius (I)	−0.74	−4.38	0.99

TABLE 2. Segment mass and inertial parameters.

Bone segments	Bone length (cm)	Segment mass (kg)	Segment mass center (cm)	Segment inertias (kg-cm^2)	
				It	Il
Humerus	30.000	1.790	13.080	132.080	16.690
Ulna	25.200	0.545	10.360	28.170	3.480
Radius	23.300	0.545	9.720	28.170	3.480
Hand	18.500	0.460	4.300	28.290	4.070

The VM requires a large set of morphometric and architectual parameters including muscle mass (M_m), optimal fascicle length (L_{ce0}), maximum musculotendon length (L_{mt}^{max}), optimal tendon length (L_{se0}), and the fraction of fiber type distribution (Tables 3 and 4). The muscle mass determines the maximum tetanic isometric force (F_0) of the muscle:

$$F_0 = \frac{M_m \varepsilon}{\rho L_{ce0}} \quad (1)$$

with zero pennation angle, constant muscle density ($\rho = 1.06$ g/cm^3) and specific tension ($\varepsilon = 31.8$ N/cm^2). The virtual muscle model uses L_{se0} (the tendon length at maximal tetanic isometric force) instead of tendon slack length, or L_{ses},[52] since L_{ses} is less well defined than L_{se0} and tends to be about 5% shorter than L_{se0}, which was estimated as[10]:

$$L_{se0} = 1.05 * L_{ses} \quad (2)$$

The steps used to determine muscle architectural parameters in VM model were given as follows:

1. L_{mt}^{max} for each muscle element was estimated from musculoskeletal model in SIMM. The measurements made within planar range of joint motion may under estimate the true values of L_{mt}^{max}. However, this parameter can be tuned to maximize the force production capacity of muscles in different applications.
2. Initially, L_{ce0} and L_{ses} were obtained from literature[24] for each muscle, and then L_{se0} was calculated by Eq. (2). Once L_{mt}^{max}, L_{ce0}, and L_{se0} were given, the operating range of the normalized muscle fascicle length ($\bar{L}_{ce} = L_{ce}/L_{ce0}$) operating range were then

TABLE 3. Muscle architectural parameters.

Muscle	Abbreviation	Maximum musculo-tendon length L_{mt}^{max} (cm)	Muscle mass M_m (g)	Peak force F_0 (N)	Optimal fascicle length L_{ce0} (cm)	Optimal tendon length L_{se0} (cm)
Shoulder						
Deltoid						
Anterior	DA	21.07	420.93	1147.99	11.00	10.50
Posterior	DP	18.37	122.36	265.99	13.80	4.20
Supraspinatus	SS	14.68	120.87	490.00	7.40	7.50
Infraspinatus	IS	16.06	413.37	1203.99	10.30	5.60
Pectoralis major						
Clavicular	PC	18.06	206.27	363.99	17.00	0.40
Elbow						
Biceps						
Long	Blh	40.54	335.99	629.99	16.00	24.50
Short	Bsh	38.13	311.03	434.00	21.50	15.50
Triceps						
Lateral	Tlt	26.54	285.60	611.17	13.60	13.00
Long	Tlh	38.85	452.20	763.49	17.00	22.00
Medial	Tmd	18.69	193.20	629.99	9.20	9.56
Brachialis	BS	16.66	341.27	994.27	10.30	6.60
Brachioradialis	BR	30.57	177.33	265.93	20.00	11.00
Major forearm						
Pronator teres	PT	15.92	91.47	560.00	4.90	11.51
Pronator quadratus	PQ	5.22	10.20	76.50	4.00	1.20
Supinator	SP	6.97	66.01	476.00	4.16	2.94

| Muscle | Fractional PCSA (%) | | | Number of motor units | | |
| | Johnson *et al.* (1972) | | | | | |
	SS	S	F	SS	S	F
Shoulder						
Deltoid						
Anterior	0.0	0.6	0.4	0.0	3.0	3.0
Posterior	0.0	0.6	0.4	0.0	3.0	3.0
Supraspinatus	0.0	0.6	0.4	0.0	3.0	3.0
Infraspinatus	0.0	0.6	0.4	0.0	3.0	3.0
Pectoralis major						
Clavicular	0.0	0.4	0.6	0.0	2.0	4.0
Elbow						
Biceps						
Long	0.0	0.3	0.7	0.0	2.0	4.0
Short	0.0	0.5	0.5	0.0	2.0	3.0
Triceps						
Lateral	0.0	0.5	0.5	0.0	2.0	3.0
Long	0.0	0.3	0.7	0.0	2.0	3.0
Medial	0.0	0.5	0.5	0.0	2.0	3.0
Brachialis	0.0	0.5	0.5	0.0	2.0	3.0
Brachioradialis	0.0	0.4	0.6	0.0	2.0	3.0
Major forearm						
Pronator teres	0.0	0.5	0.5	0.0	2.0	3.0
Pronator quadratus	0.0	0.5	0.5	0.0	2.0	3.0
Supinator	0.0	0.5	0.5	0.0	2.0	3.0

determined by the internal algorithm in VM.[10] Based on desired $\bar{L}_{ce}$ operating range, the initially chosen L_{ce0} and L_{se0} could be inversely determined through trial-and-error methodology and adjusted at the same time to lie in the tolerable range of empirical measured values. In our VA model development, since muscles operate mostly in the ascending part of the length–tension curve in the vicinity of L_{ce0}, the initially chosen L_{ce0} and L_{se0} were adjusted so that $\bar{L}_{ce}$ is constrained by $0.45 \leq \bar{L}_{ce} \leq 1$ in the full range of joint motion.

3. F_0 for each of the 15 muscles were based on literature.[24] Then M_m was calculated using Eq. (1).

4. The percentage of fiber distribution for slow- and fast-twitch types was obtained from literature[25] for the shoulder and elbow muscles. For forearm muscles, no data on fiber type distribution are available in literature. Thus, an even distribution of fiber type was assumed between slow- and fast-twitch fiber types. The total number of motor units included in each muscle ranged from 5 to 7, in order to achieve relatively smooth force recruitment without a heavy computational burden for simulation.

Implementation of Proprioceptor Models

We implemented the muscle spindle model developed previously[37] in a Simulink S-function block shown in Fig. 3a. The spindle model is composed of three intrafusal fiber types, i.e., bag1, bag2, and chain fibers. Each spindle model has three inputs: fascicle length (L_{ce}), static (γ_{stat}), and dynamic (γ_{dyn}) fusimotor drives, and two outputs representing activity in type I_a and type II sensory neurons.

In the original spindle model,[37] the two fusimotor inputs, γ_{stat} and γ_{dyn}, are represented by the firing frequency (Hz) of activation, which are converted to an activation level between 0 and 1 for each intrafusal fibers within the spindle model. In the current implementation, the conversion from frequency to activation is replaced by directly using activation levels from 0 to 1 for γ_{stat} and γ_{dyn} inputs to the spindle model (Fig. 3b). Because γ_{dyn} modulates the sensitivity of the bag1 fiber only, the activation level of bag1 fiber is directly equal to γ_{dyn}. However, bag2 and chain fibers receive the same γ_{dyn} input, but saturate at different firing frequencies ($f_{bag2} = 100$ Hz; $f_{chain} = 200$ Hz), the scaling relation between γ_{stat} drive and activation level saturates first at $\gamma_{stat} = 0.5$ for the bag2 fiber, then at $\gamma_{stat} = 1.0$ for the chain fiber (Fig. 3b).

The spindle model adopted in this VA system was validated by a large set of experimental data in Mileusnic *et al.*[37] Our implementation using a Simulink S-function block makes the model numerically more efficient in computation and can be inserted into multi-muscle systems modeled in the Matlab/Simulink environment. The values of model parameters for the spindle were taken from those fitted by experimental data used in
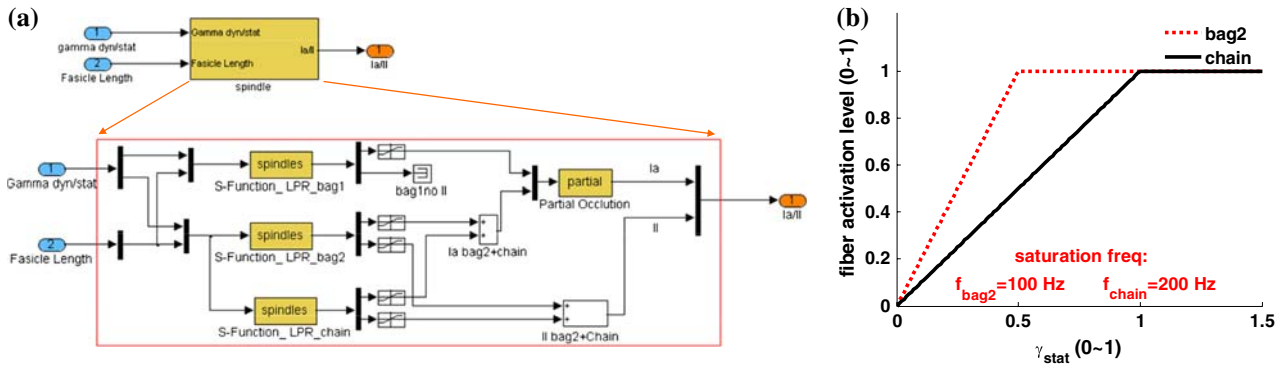
(a)

(b)

FIGURE 3. S-function implementation of the spindle model. (a) Matlab/Simulink S-function implementation of each intrafusal fibers in the spindle model. The spindle model which consists of three intrafusal fiber models (bag1, bag2, chain); two afferent firing summation nodes (I_a/II afferent firing models); and the partial occlusion effect in primary afferent firing. Each intrafusal fiber model responds to two inputs: fascicle length and the relevant fusimotor drive. The spindle model generates two outputs: I_a and II afferent activity. (b) Frequency-to-activation conversion and saturation effect for bag2 and chain fibers. The S-function spindle model skips the frequency-to-activation conversion in the original model by directly scaling the gamma static commands (γ_{stat}) for bag2 and chain fibers according to their different saturation frequencies. Receiving the same γ_{stat} drive (0–1), bag2 saturate at 0.5 corresponding to its saturation frequency of 100 Hz, whereas chain fiber saturate at 1, corresponding to its saturation frequency of 200 Hz.

Mileusnic et al.[37] Simulation of the S-function spindle block with the set of inputs identical to those in Mileusnic et al.[37] verified the correct implementation of the spindle model. The outputs of the S-function spindle model gave the same patterns of primary and secondary firings as produced in.[37]

We used a piece-wise linear static relation (Fig. 4) between the total muscle force and I_b afferent firing to account for the ensemble response of the GTO in the muscle. The higher slope at the lower levels of muscle
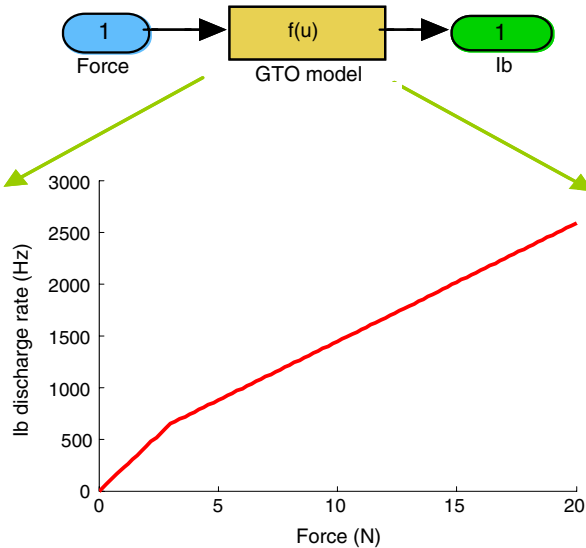

FIGURE 4. Simulink implementation of a GTO model representing piece-wise linear static relation between the total muscle force and I_b afferent firing to account for the ensemble response of the GTO in the muscle. The higher slope at the lower levels of muscle forces is due to the recruitment of tendon organs, which makes the predominant contribution to the total response at low forces.

forces is due to the disproportionate influence of the early-recruited slow-twitch muscle fibers to GTO output.[13,38]

Model Integration in Matlab/Simulink

Integration of individual model components, such as the VM, the spindle model, the GTO model and the skeletal SIMM model, was accomplished using a software tool—musculoskeletal modeling in simulink (MMS).[14] MMS is a C program that automatically converts a SIMM model of a sensorimotor system into a Simulink block that embodies its mechanical dynamics. The dynamics pipeline module of SIMM calls for SD/FAST to generate the set of equations of motion for the skeletal model, which is in turn converted into a kinetics block in Simulink by the MMS. The virtual muscle blocks are then interfaced with the kinetics block to effect joint movements. The MMS connects the spindle and GTO models with muscle fascicle lengths and forces. The α and γ commands are scaled neural inputs (0–1) to muscles and spindles respectively. The outputs are joint kinematics (q, $\dot{q}$, $\ddot{q}$), muscle activations (u), muscle forces (F_m), musculo-tendon lengths (L_{mt}), and the ensemble activity levels of spindle primary (I_a) and secondary (II) GTO (I_b) proprioceptors.

Dynamic Simulation Using the VA model

The integrated sensorimotor VA was validated in the full range of muscle (α) and spindle (γ) commands with open-loop simulations. In the validation study, the forearm DOF was constrained at zero degree, leaving only two DOFs for the shoulder horizontal

F/E and elbow F/E. Muscles selected here included DP and Pectorailis Major (Clavicle portion, PC) for mono-articular shoulder joint muscles; Brachialis (BS) and Triceps lateral (Tlt) for mono-articular elbow joint muscles; and Biceps short (Bsh) and Triceps long (Tlh) as bi-articular muscles. The choice of this "subset" muscles was based on that: (1) a large number of experiments were performed with the similar joint configuration[8,21,41]; and (2) two pairs of mono-articular muscles and one pair of bi-articular muscles were commonly adopted in previous simulation approaches investigating multi-joint arm reaching movements.[16,23,27,42]

In the first set of simulations, three patterns of open-loop α commands were selected to achieve three equilibrium hand positions in the workspace (A, B and C in Fig. 8a). At each hand position, additional five patterns of increasing muscle activation were then tuned to maintain the same equilibrium hand position with higher stiffness. In these simulations, constant spindle fusimotor inputs ($\gamma_{stat} = \gamma_{dyn} = 0.3$) were used to drive the spindle.

One of the purposes of developing such a comprehensive model for sensorimotor system is to investigate the roles of muscle proprioceptive feedback in multi-joint arm posture and movement control. The second set of simulations was designed to demonstrate the modulating effects of fusimotor drive to spindle primary (I_a) and secondary (II) afferents. Therefore, simulations were carried out with six incremental levels of γ commands ($\gamma_{stat} = \gamma_{dyn}$) to muscle spindles at each of the three hand positions, respectively. At a fixed hand position, any change in spindle I_a and II firings would be due to the modulating effects of increased fusimotor commands. These simple open-loop simulations were designed to distinguish the effects of different factors on the sensorimotor responses, thus validating the VA model without undue complexity in the interpretation of simulation results.

RESULTS

Parameterizing the VA Model

The VA model is the integration of the four sub-components of sensorimotor system: the musculoskeletal model, the VM, and the muscle spindle and the GTO models. Accurate parameterization will ensure proper operation of the VA model in simulation. The choice of parameters is not tailored to subject specific information, but rather is based on measurement values available in literature. However, this will provide a template of parameters for further specification.

The torque generating capacity of muscles within the range of joint motion is the most important feature of the musculotendon unit, which is given by their moment arm profiles in Fig. 5. For shoulder muscles, i.e., PC, DA, DP, SS and IS in Fig. 5a, the solid lines show the SIMM generated moment arm profiles that demonstrate a good fit to experimental profile[26] in a large range of motion. Discrepancy in the extreme regions of joint motion may be attributed both to measurement errors and limitation of SIMM to capture complex musculotendon geometry. However, the peak moment arms of these shoulder muscles are matched well to the measured values, suggesting that the model is able to replicate muscle capacity of moment generation in the large range of shoulder movement. There is a paucity of information on moment arm data available for both heads of biceps and long head of triceps at the shoulder joint.[49] Their moment arm profiles are adjusted to match one measured value in Fig. 5a. The single point experimental value of moment arm indicated by a star falls closely to the moment arm profile from SIMM (solid red line) of the biceps (short head) at the shoulder joint. For elbow muscles in Fig. 5b, SIMM generated moment arm profiles (solid lines) fit very well with those of experimental measurements (dotted lines).[40] Similarly good fit is obtained for all forearm muscles (Fig. 5c) based on the data in Haugstvedt et al.[22] It is noted that the biceps have a significant supination action at the forearm. Therefore, activation of the biceps will produce significant actions on the forearm, elbow and shoulder joints. Such coupled actions cross multiple joints will have an important implication on the functional use of the biceps in motor tasks.

A large set of parameters for each component model was adopted from literature.[13,24,25,37,44,48] Tables 2–4 list the parameter values of limb segment, muscle architecture and fiber fractional distribution used in the VA model. Among the parameters, muscle architectural parameters must be tuned, so that the muscles operate in the region, in which their normalized fascicle lengths ($\bar{L}_{ce}$) are constrained to $0.45 \leq \bar{L}_{ce} \leq 1$. Figure 6 confirms that the procedure we used to fine-tune muscle parameters (see Methods, Section "Virtual Muscle Model Parameters") does yield normalized fascicle length that falls within this pre-specified range. Thus, it ensures that the muscles are operating in the ascending part of their length–tension relationship with positive intrinsic stiffness. Muscle architectural parameters that are finally tuned in this model are comparable to those reported in literature, and are within their physiological ranges (see Tables 5–7 in the Appendix A).

Dynamic Validation of the VA Model

The dynamic behavior of the VA model was evaluated with simple patterns of open-loop activation.
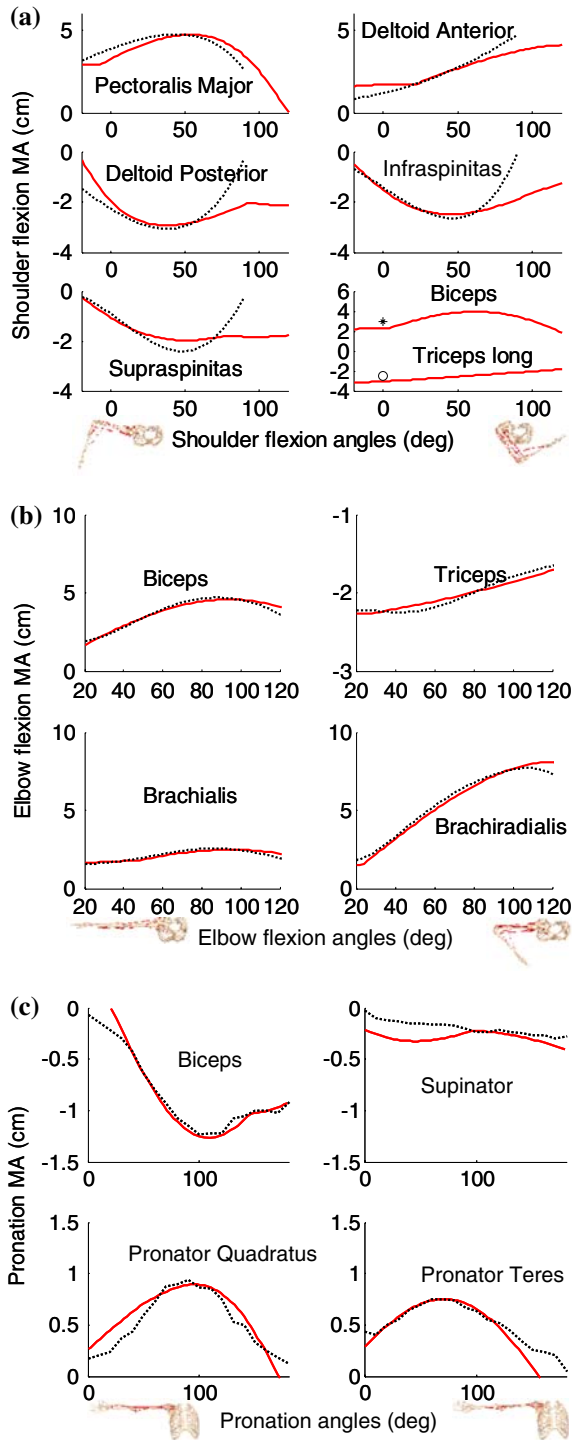
FIGURE 5. Moment arm matching of shoulder flexion and extension (F/E) (a), elbow F/E (b), and forearm pronation and supination (P/S) (c). The dotted lines are the experiment measurements, the solid lines are from SIMM model. The muscle paths are validated through matching the model moment arm profiles of shoulder, elbow and forearm joints with those obtained from experimental measurements. Since the shoulder F/E moment arms of two heads of biceps and the long heads of triceps muscles are only measured at one single joint configuration, the model moment arm profiles are compared to the single data points in (a).
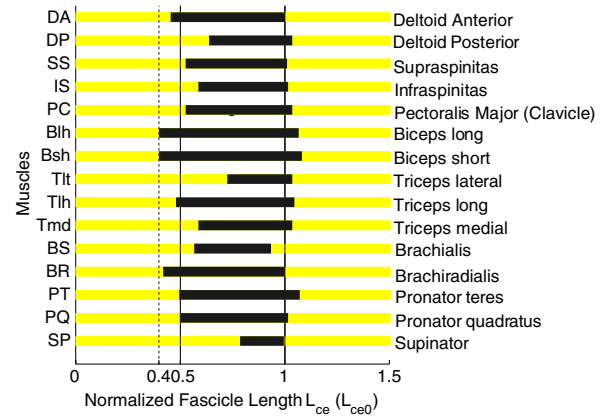

FIGURE 6. Diagram showing the operating range of fascicle length (L_{ce}) predicted for each muscle in the VA model. The left and right edges of each dark bar indicate the values of $\bar{L}_{ce}^{min}$ and $\bar{L}_{ce}^{max}$ corresponding to the minimum and maximum physiological lengths of each musculotendon elements respectively, and the dark bars illustrate the portions of the length–tension curve on which muscle develops active force.

Figure 7 illustrates an example of dynamic responses with open-loop constant α and γ inputs ($\gamma_{stat} = \gamma_{dyn} = 0.3$). It is shown that both the shoulder and elbow joints are stabilized quickly after an initial oscillation, because of the inherent stability of the neuromuscular system. The hand converges to a position in workspace (i.e., position C in Fig. 8a). The responses of internal variables of the system, such as muscle force (F_m), musculotendon length (L_{mt}), fascicle length (L_{ce}), and sensory responses of I_a, I_b and II afferents, reveal that their dynamic and steady state values are all within physiological ranges. This indicates that the model dynamics are propagating in time throughout the system from muscle (α) and spindle (γ) inputs to the output of arm configuration within the biomechanical and physiological constraints.

Sensory responses of spindle and GTO at steady state are verified under different sets of open-loop simulations, in which the hand of the arm is positioned to three positions (A, B, and C in Fig. 8a) in space. In these simulations, when fusimotor drives are kept constant ($\gamma_{stat} = \gamma_{dyn} = 0.3$), the I_a and II firing frequencies display an insignificant change (SD/mean < 10%) for all increasing α commands in each hand position (data not shown here). This is due to trivial changes in muscle fascicle lengths with increasing muscle activations when the hand position is fixed. It also implies that the serial elastic component of tendon has an insignificant effect on spindle afferent encoding of joint angle. However, I_a and II firings exhibit a strong dependency on hand positions in space and muscle fascicle lengths. This is depicted in Fig. 8b, in which I_a and II firing rates (the left axis) and fascicle lengths (L_{ce}) (the right axis) are plotted against the
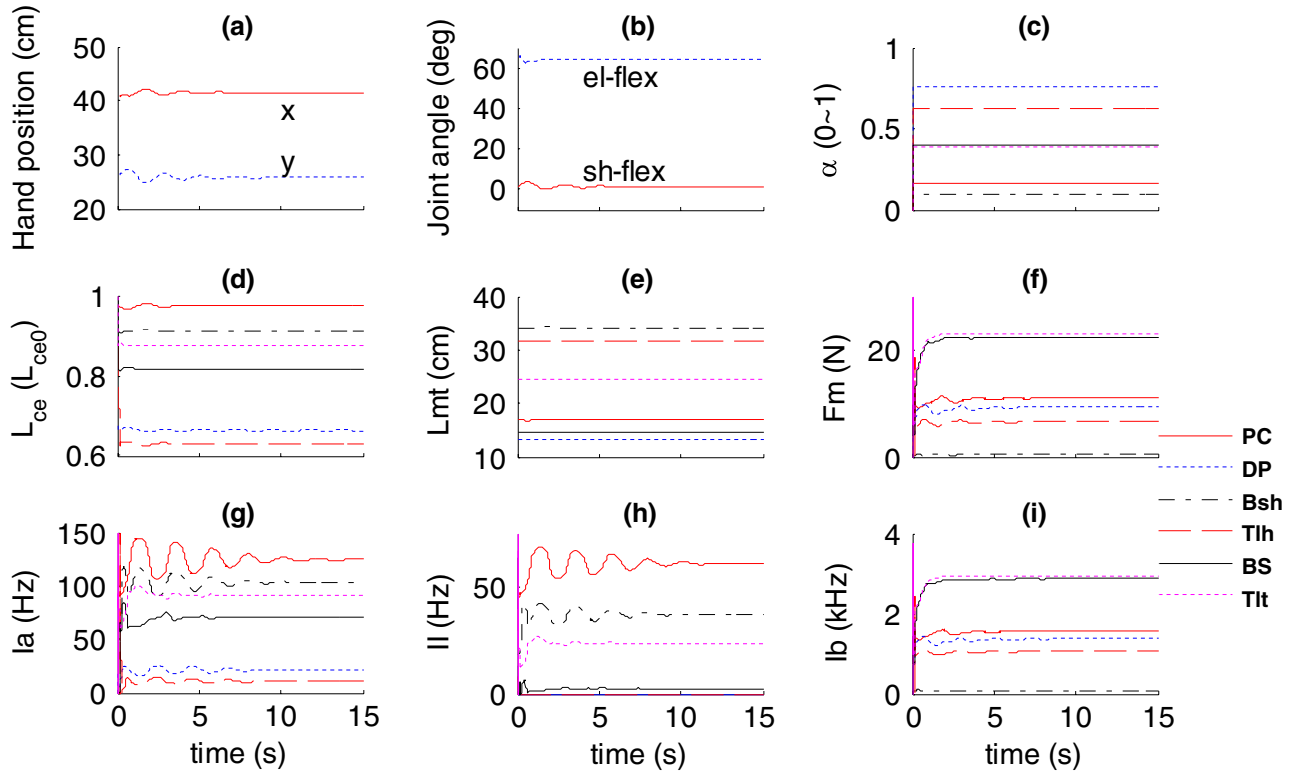
FIGURE 7. Dynamic responses of one simulation at hand position C: (a) hand kinematics in the Cartesian coordinate originated at shoulder, (b) shoulder and elbow joint kinematics, (c) α command of the six muscles, (d) L_{ce}, and (e) L_{ce}, (f) muscle force F_m, (g) spindle I_a and (h) II firings, and (i) GTO I_b firings of 6 muscles.
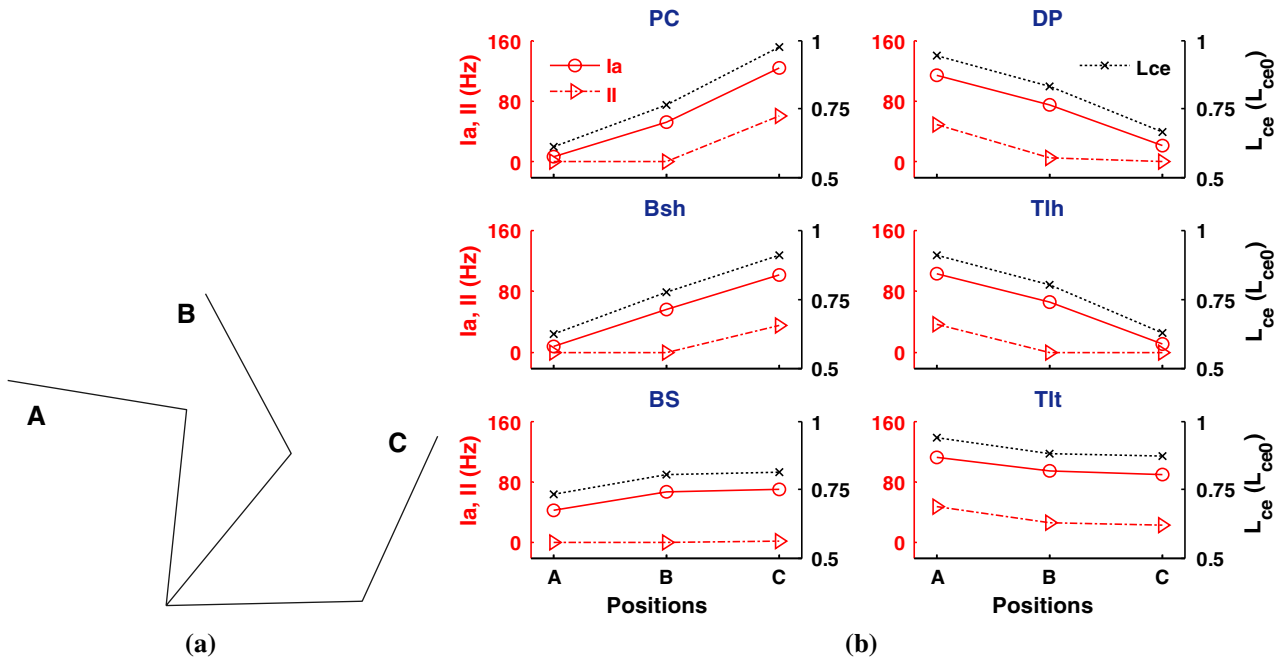

FIGURE 8. (a) Three hand positions (A, B, C) in space achieved with three sets of open-loop activations. (b) With the constant fusimotor drives ($\gamma_{stat} = \gamma_{dyn} = 0.3$), the steady state values of I_a and II firings (left axis, red) and muscle fascicle lengths (right axis, black) are shown at the three hand positions (A, B, and C) in the workspace. Each plot is for one of the six muscles. There is a monotonic relation between afferent firings with the arm positions and muscle fascicle lengths.
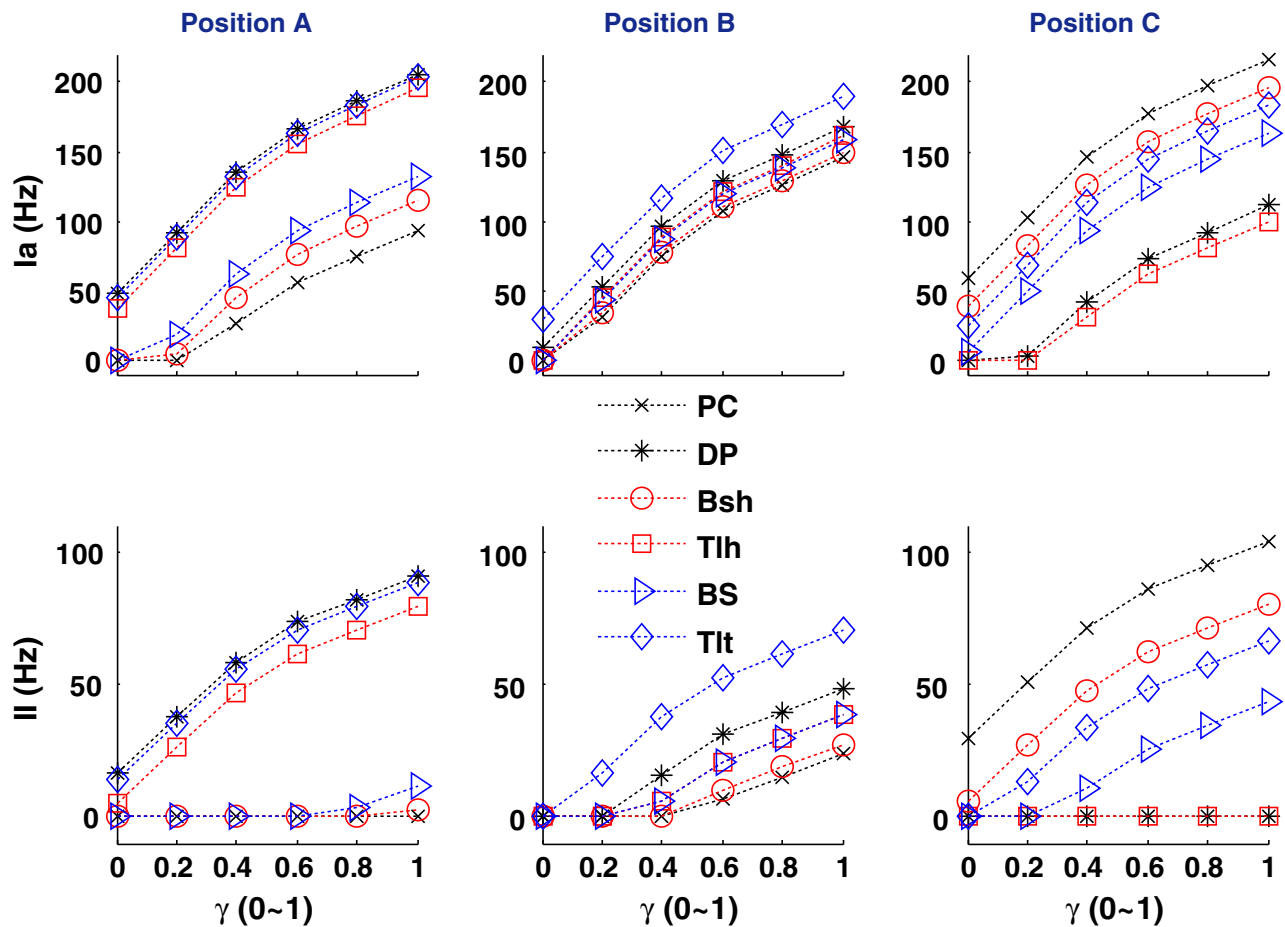
FIGURE 9. The relation between equilibrium I_a (1st row) and II (2nd row) firing with γ ($\gamma_{stat} = \gamma_{dyn}$) activations for the six muscles at the three workspace locations (A, B, and C). The figure demonstrates that once the primary and secondary afferents were activated, the firing frequency shows a monotonic relationship with the fusimotor drives at all of the three hand positions.

three hand positions for the six muscles. Such monotonic correlation suggests a plausible mechanism for the CNS to encode hand positions in the workspace by spindle afferents.[43,47] At the three hand positions, however, when fusimotor drives are increased from 0 to 1, spindle I_a and II afferents display a strong modulation by the γ drives (Fig. 9). The monotonic increase in I_a and II firings with increasing fusimotor drives at the three hand positions illustrates an effective modulation of spindle afferents by the γ commands in the model. Thus, γ fusimotor drive has a significant effect on spindle afferent encoding of joint angle, which should be taken into consideration in the encoding and decoding of joint angle from spindle afferents.

DISCUSSION

We are taking an integrative approach to modeling a multi-muscle, multi-joint, sensorimotor system of the human arm. Realistic component models of muscles and proprioceptors that are developed and validated previously have been integrated into a larger systems model in the Matlab/Simulink environment. This environment facilitates addition of models of neural controllers that have been hypothesized to account for experimentally observed movements and behaviors. The modular approach eases further development, improvement, maintenance and exchange of model components, and updating of model parameters based on new experimental data. The ability of a systems level model to replicate physiological phenomena with anatomically realistic components and parameters effectively "closes the loop" on a modeling process that can appear to be arbitrary when viewed from the limited perspective of individual components and subsystems. Systems models are beginning to demonstrate its usefulness in the analysis of neural control of motor behaviors.[30] The realistic features of the VA model developed and validated here further support its

validity as a tool for computational studies of motor control in parallel with experimental approaches.

The realistic feature of the VA is greatly enhanced by the digitized bony structure of the upper arm,[24] which provides a realistic constraint to muscle attachments and mechanical actions on joints. With such anatomical constraint, we are able to match muscle moment arms at joints of span to available experimental data closely (Fig. 5). Wrapping surfaces and path constraints are useful to define musculotendon paths, so that they do not cut into the bone surface. The profiles of muscle moment arm (MA) can be matched closely to those of experimental measurements by adjusting muscle insertion points and musculotendon paths. Results in Fig. 5 may be the best match we could achieve with a line representation of the musculotendon path. More realistic representation of musculotendon path will await 3D modeling of muscle geometry.[3] The choice of muscles included in this model is dictated by the availability of experimental data in moment arm and architectural parameters. The anatomical structure of the arm in this model represents an average size of human upper extremity, and a subject specific model may be developed by scaling the average model to match the size of a specific subject.

Another major realistic feature is the incorporation of the virtual muscle[TM] (VM) model[10] to the VA model. The VM model is capable of modeling three types of muscle fibers, i.e., slow twitch (or fatigue), fast twitch (or fatigue) and slow-fatigue-fast twitch. The relative portion of each fiber type in the whole muscle can be specified. A linear combination of recruitment and frequency modulation scheme that is built in the VM model mimics the physiologic order of recruitment according to the size principle of the spinal motoneurons. Each fiber type has a similar structure of activation and contraction dynamics, but with a different set of parameter values for different twitch speeds fitted from a series of experiment measurements.[4–7] In addition, the phenomena of muscle yielding, sag, rise and fall times in activation that have not been considered in previous muscle models are included in the VM model. These physiologic properties of muscle fibers make the VM the most realistic muscle model currently available. With its built-in recruitment scheme in the VM, a lumped motoneuron pool at the spinal cord can be used to represent the "final common path" of motor outputs from the CNS to muscle actuators.

The third important feature of the VA model is the integration of proprioceptor models into the virtual muscle. Particularly, the physiologically realistic spindle model[37] used here includes the delicate structures and properties of a mammalian muscle spindle. Three types of intrafusal fibers (bag1, bag2, and chain) are modeled

and parameters are fitted to a large set of experimental data. The intrafusal fibers are innervated by γ_{stat} and γ_{dyn} inputs, and their outputs are combined to give rise to the primary (I_a) and secondary (II) afferents. In the model, a range of continuous modulation of fusimotor activity (from 0 to 1) is used to control the static and dynamic sensitivities of the spindle to length and velocity changes. This would allow investigation of biologically plausible roles of fusimotor control in motor task performance. In human muscles, a large number of spindles may be recruited in order to increase the range of length sensitivity.[11] However, this lumped spindle model[37] has been calibrated using ensemble firing patterns recorded in animals to represent the collective response of a set of spindles. The continuous static and dynamic fusimotor drives to the lumped spindle model may be equivalent to the outputs from γ motoneurons in the spinal cord. In this sense, fusimotor control of spindle model will allow further investigation in proprioceptive control of multi-joint posture and movement.

The VA model also produced consistent results in spindle afferents with respect to γ fusimotor control (Fig. 9) and muscle fascicle length (or hand position) change (Fig. 8). Sensory responses (Fig. 9) suggest that γ_{stat} and γ_{dyn} are generally effective in modulating I_a and II firing rates of the spindle model. Figure 9 shows the monotonic relation between spindle I_a, II firings and muscle fascicle lengths (or hand positions) in the six muscles at different hand positions. The fact that spindle afferents vary proportionally with changes in fascicle length lends a direct support to the hypothesis that end-point positions of a multi-joint limb can be decoded from proprioceptive information originating from different muscles.[43,47] However, the secondary afferent is more susceptible to unloading at short muscle length than the primary afferent, as seen in position A for BS and Bsh muscles and in position C for DP and Tlh muscles (Fig. 8). Thus, primary afferent would be more reliable to indicate muscle fiber length than secondary afferent. The results also indicate that if primary afferents of multiple muscles are used to encode or decode joint (or hand) positions of the arm, the effect of γ efferent to spindle must be taken into account. Furthermore, we noticed that at a fixed hand position, muscle fibers are maintained at roughly constant lengths even when α commands increased substantially for each muscle. This is also a result of stiff series elastic component of the tendon. It indicates that spindle afferents remain nearly unaffected by increasing α commands. In other words, tendon elasticity may be a negligible factor in encoding or decoding joint and hand positions from spindle afferents.

In applications, the VA model may be further tuned to suit simulation of specific tasks. The operating range

of muscle length–tension property chosen in this study may not reflect the best functional range for a specific task, since we are mainly concerned here with validating the input-output behaviors of the VA model. Restricting muscles to operate in the ascending limb of their length–tension curve (i.e., $0.45 \le \bar{L}_{ce} \le 1$) may be stringent for motor task control. We have relaxed this condition in a postural control task.[45] It was demonstrated that a larger range of postural angles can be reached with same descending commands and spinal reflex gains, if a wider range of length–tension curve in the muscles is specified. Thus, in a task simulation, tuning muscle length–tension curves to obtain an optimum functional setting would further enhance the utility of the VA model.

The VA model developed in this study is able to replicate a wide range of sensorimotor responses with simple patterns of open-loop, α and γ motor commands. The VA model represents a complete sensorimotor system that translates neural commands to the actuation forces (muscle model), the sensory afferents (spindle and GTO models), the multi-joint dynamics (skeletal model), and the ultimate motor behaviors at the hand. This neuromotor process produces a full set of physiologic variables that may correspond to those that are measurable in experiments (e.g., joint kinematics, joint torque/stiffness and hand force/stiffness, etc.), and also those that are not accessible to invasive instruments (fascicle lengths, muscle force, fusimotor drives, etc.). In future studies, we will use this VA model to address

motor control issues that have not been completely elucidated with data from human behavioral experiments. The model may also be expanded, or modified, to represent various neuropathologic conditions, such as deafferentation, stroke and spinal cord injury, and to address the strategies of neuro-rehabilitation.

APPENDIX A

The muscle architectural parameters of each of the 15 muscles in the VA model were tuned step by step as described in Methods, Section "Virtual Muscle Model Parameters". The physiological constraint for this tuning process is the fascicle length operating range within $0.45 \le \bar{L}_{ce} \le 1$ (See Fig. 6). At the same time, there has been a wide range of literature reports on muscle peak force (F_0), optimal fascicle length (L_{ce0}), and tendon slack length (L_{ses}). We compared the values of our VM parameters with those of experimental measurements and previous modeling approaches here in Table 5 on F_0, Table 6 on L_{ce0} and Table 7 on L_{ses}. There is a large variability in the literature on each of the three sets of parameters due to the possible differences in experimental preparations and specimen size.[17,18,20,24,33,39] However, our model parameters fall generally within the range of physiological values, and the VA model reproduces the realistic force generating capability of human arm muscles.

TABLE 5. comparison of muscle peak forces with literature values.

Muscle	Peak force F_0 (N)				
	Model	Holzbaur[24]	Garner[18]	Garner[17]	Gonzalez[20]
Shoulder					
Deltoid					
Anterior	1147.99	1142.60		277.48	
Posterior	265.99	259.90		567.15	
Supraspinatus	490.00	487.80	687.99	687.84	
Infraspinatus	1203.99	1210.80	1100.13	1099.61	
Pectoralis major					
Clavicular	363.99	364.40		342.46	
Elbow					
Biceps	1063.99		849.29		143.00–251.00
Long	629.99	624.30		461.76	
Short	434.00	435.60		392.91	
Triceps	2004.65		2332.92		279.00–1040.00
Lateral	630.00	624.30		1268.87	
Long	798.00	798.50		629.21	
Medial	629.99	624.30		619.67	
Brachialis	994.00	987.30	853.76	853.90	183.00–588.00
Brachioradialis	266.00	261.30	101.56	101.58	93.00–200.00
Major forearm					
Pronator teres	560.00	566.20	592.31	592.80	
Pronator quadratus	76.50	75.50			
Supinator	476.00	476.00	186.36	186.38	

TABLE 6. Comparison of optimal fascicle lengths with literature values.

Muscle	Optimal fascicle length L_{ce0} (cm)						
	Model	Holzbaur[24]	Garner[18]	Garner[17]	Langerderfer[33]	Murray[39]	Gonzalez[20]
Shoulder							
Deltoid			12.80				
Anterior	11.00	9.76		14.68	10.12(0.30)		
Posterior	13.80	13.67		17.02	14.18(2.52)		
Supraspinatus	7.40	6.80	4.28	4.28	7.07(0.40)		
Infraspinatus	10.30	7.60	6.76	6.76	8.74(2.46)		
Pectoralis major			19.00				
Clavicular	17.00	14.42		22.65	14.95(3.10)		
Elbow							
Biceps			14.22				14.30–15.30
Long	16.00	11.60		15.36	15.61(0.30)	12.8(3.20)	
Short	21.50	15.00		13.07	18.09(0.38)	14.5(3.20)	
Triceps			8.77				6.70–14.50
Lateral	13.60	11.40		6.17	10.28(2.44)	9.30(2.80)	
Long	17.00	13.40		15.24	17.62(1.05)	12.70(2.10)	
Medial	9.20	9.20		4.90	14.46(0.87)		
Brachialis	10.30	9.00	10.28	10.28	9.42(2.32)	9.00(1.60)	9.00–18.50
Brachioradialis	20.00	16.40	27.03	27.03	17.53(1.79)	17.70(3.00)	14.20–23.00
Major forearm							
Pronator teres	4.90	4.90	4.48	4.48		5.50(1.20)	
Pronator quadratus	4.00	2.83					
Supinator	4.16	3.30	6.04	6.04			

TABLE 7. Comparison of tendon slack length with literature values.

Muscle	Tendon slack length L_{ses} (cm)						
	Model	Holzbaur[24]	Garner[18]	Garner[17]	Langerderfer[33]	Murray[39]	Gonzalez[20]
Shoulder							
Deltoid			5.38				
Anterior	10.00	9.30		1.64	2.60(2.30)		
Posterior	4.00	3.80		5.93	4.00(0.80)		
Supraspinatus	7.14	4.00	13.03	13.03	2.95(0.65)		
Infraspinatus	5.33	3.10	5.58	5.58	5.08(0.13)		
Pectoralis major			6.35				
Clavicular	0.38	0.30		0.45	2.28(0.68)		
Elbow							
Biceps			22.98				21.00
Long	23.33	27.20		22.93	18.28(1.38)	22.90(1.60)	
Short	14.76	19.20		22.98	15.75(0.85)	18.30(2.50)	
Triceps			19.05				18.38
Lateral	12.38	9.80		19.64	16.70(0.65)	18.70(1.80)	
Long	20.95	14.30		19.05	19.95(0.60)	21.70(2.90)	
Medial	9.10	9.10		12.19	17.80(1.13)		
Brachialis	6.29	5.40	1.75	1.75	3.35(0.45)	11.60(1.30)	4.52
Brachioradialis	10.48	13.30	6.04	6.04	10.35(0.5)	16.9(1.7)	12.60
Major forearm							
Pronator teres	10.96	9.80	11.58	11.58		12.00(1.60)	
Pronator quadratus	1.14	0.50					
Supinator	2.80	2.80	2.48	2.48			

REFERENCES

[1] Abend, W., E. Bizzi, and P. Morasso. Human arm trajectory formation. *Brain* 105:331–348, 1982.

[2] Alstermark, B., N. Lan, and L.-G. Pettersson. Building a realistic neuronal model that simulates multi-joint arm and hand movements in 3D-space. *HFSP Journal* 1(4):209–214, 2007.

[3] Blemker, S. S., and S. L. Delp. Three-dimensional representation of complex muscle architectures and geometries. *Ann. Biomed. Eng.* 33:661–673, 2005.

[4] Brown, I. E., E. J. Cheng, and G. E. Loeb. Measured and modeled properties of mammalian skeletal muscle. II. The effects of stimulus frequency on force–length and force–velocity relationships. *J. Muscle Res. Cell Motil.* 20:627–643, 1999.

[5] Brown, I. E., and G. E. Loeb. Measured and modeled properties of mammalian skeletal muscle. I. The effects of post-activation potentiation on the time course and velocity dependencies of force production. *J. Muscle Res. Cell Motil.* 20:443–456, 1999.

[6] Brown, I. E., and G. E. Loeb. Measured and modeled properties of mammalian skeletal muscle: III. The effects of stimulus frequency on stretch-induced force enhancement and shortening-induced force depression. *J. Muscle Res. Cell Motil.* 21:21–31, 2000.

[7] Brown, I. E., and G. E. Loeb. Measured and modeled properties of mammalian skeletal muscle: IV. Dynamics of activation and deactivation. *J. Muscle Res. Cell Motil.* 21:33–47, 2000.

[8] Burdet, E., R. Osu, D. W. Franklin, T. E. Milner, and M. Kawato. The central nervous system stabilizes unstable dynamics by learning optimal impedance. *Nature* 414:446–449, 2001.

[9] Capaday, C., and J. D. Cooke. Vibration-induced changes in movement-related EMG activity in humans. *Exp. Brain Res.* 52:139–146, 1983.

[10] Cheng, E. J., I. E. Brown, and G. E. Loeb. Virtual muscle: a computational approach to understanding the effects of muscle properties on motor control. *J. Neurosci. Methods* 101:117–130, 2000.

[11] Cordo, P. J., C. Flores-Vieira, S. M. P. Verschueren, J. T. Inglis, and V. Gurfinkel. Position sensitivity of human muscle spindles: single afferent and population representations. *J. Neurophysiol.* 87:1186–1195, 2002.

[12] Cordo, P., S. C. Gandevia, J. P. Hales, D. Burke, and G. Laird. Force and displacement-controlled tendon vibration in humans. *Electroen. Clin. Neurophysiol.* 89:45–53, 1993.

[13] Crago, P. E., J. C. Houk, and W. Z. Rymer. Sampling of total muscle force by tendon organs. *J. Neurophysiol. (Bethesda)* 47:1069–1083, 1982.

[14] Davoodi, R., I. E. Brown, N. Lan, M. Mileusnic, and G. E. Loeb. An integrated package of neuromusculo-skeletal modeling tools in SimulinkTM. In: 23rd IEEE/EMBS Ann Int'l Conf 2001.

[15] Delp, S. L., and J. P. Loan. A graphics-based software system to develop and analyze models of musculoskeletal structures. *Comput. Biol. Med.* 25:21–34, 1995.

[16] Flash, T. The control of hand equilibrium trajectories in multijoint arm movements. *Biol. Cybern.* 57:257–274, 1987.

[17] Garner, B. A., and M. G. Pandy. Musculoskeletal model of the upper limb based on the visible human male dataset. *Comput. Methods Biomech. Biomed. Eng.* 4:93–126, 2001.

[18] Garner, B. A., and M. G. Pandy. Estimation of musculotendon properties in the human upper limb. *Ann. Biomed. Eng.* 31:207–220, 2003.

[19] Ghez, C., J. Gordon, M. F. Ghilardi, C. N. Christakos, and S. E. Cooper. Roles of proprioceptive input in the programming of arm trajectories. *Cold Spring Harb. Symp. Quant. Biol.* 55:837–847, 1990.

[20] Gonzalez, R. V., E. L. Hutchins, R. E. Barr, and L. D. Abraham. Development and evaluation of a musculoskeletal model of the elbow joint complex. *J. Biomech. Eng. Trans. ASME* 118:32–40, 1996.

[21] Gordon, J., M. F. Ghilardi, and C. Ghez. Impairments of reaching movements in patients without proprioception. 1. Spatial Errors. *J. Neurophysiol.* 73:347–360, 1995.

[22] Haugstvedt, J. R., R. A. Berger, and L. J. Berglund. A mechanical study of the moment-forces of the supinators and pronators of the forearm. *Acta Orthop. Scand.* 72:629–634, 2001.

[23] Hogan, N. The mechanics of multi-joint posture and movement control. *Biol. Cybern.* 52:315–332, 1985.

[24] Holzbaur, K. R. S., W. M. Murray, and S. L. Delp. A model of the upper extremity for simulating musculoskeletal surgery and analyzing neuromuscular control. *Ann. Biomed. Eng.* 33:829–840, 2005.

[25] Johnson, M. A., J. Polgar, D. Weightman, and D. Appleton. Data on the distribution of fibre types in 36 human muscles, an autopsy study. *J. Neurol. Sci.* 18:111–129, 1973.

[26] Kuechle, D. K., S. R. Newman, E. Itoi, B. F. Morrey, and K. N. An. Shoulder muscle moment arms during horizontal flexion and elevation. *J. Shoulder Elb. Surg.* 6:429–439, 1997.

[27] Lan, N. Analysis of an optimal control model of multi-joint arm movements. *Biol. Cybern.* 76:107–117, 1997.

[28] Lan, N., and L. Baker. Biomechanical couplings between elbow and forearm movements. In: Proc. 26th IEEE/EMBS Ann. Intl. Conf., San Francisco, CA, Sept. 2004.

[29] Lan, N., and P. E. Crago. Optimal-control of antagonistic muscle-stiffness during voluntary movements. *Biol. Cybern.* 71:123–135, 1994.

[30] Lan, N., Y. Li, Y. Sun, and F. S. Yang. Reflex regulation of antagonist muscles for control of joint equilibrium position. *IEEE Trans. Neural Syst. Rehabil. Eng.* 13:60–71, 2005.

[31] Lan, N., and T. Murakata. A realistic human elbow model for dynamic simulation. In: Proc. 25th Ann. Meeting ASB, San Diego, CA, pp. 267–268, August, 2001.

[32] Lan, N., D. Song, and J. Gordon. Systems engineering approach to computational sensorimotor control. In: 28th International Symposium of Computational Neuroscience. Montréal, Canada, 2006.

[33] Langenderfer, J., S. A. Jerabek, V. I. Thangamani, J. E. Kuhn, and R. E. Hughes. Musculoskeletal parameters of muscles crossing the shoulder and elbow and the effect of sarcomere length sample size on estimation of optimal muscle length. *Clin. Biomech.* 19:664–670, 2004.

[34] Lemay, M. A., P. E. Crago, M. A. Lemay, and P. E. Crago. A dynamic model for simulating movements of the elbow, forearm, and wrist. *J. Biomech.* 29(10):1319–1330, 1996.

[35] Lin, C. C. K., and P. E. Crago. Structural model of the muscle spindle. *Ann. Biomed. Eng.* 30:68–83, 2002.

[36] Loeb, G. E., I. E. Brown, and E. J. Cheng. A hierarchical foundation for models of sensorimotor control. *Exp. Brain Res.* 126:1–18, 1999.

[37] Mileusnic, M. P., I. E. Brown, N. Lan, and G. E. Loeb. Mathematical models of proprioceptors: I. Control and

transduction in the muscle spindle. *J. Neurophysiol.* 96(4):1772–1788, 2006.

[38]Mileusnic, M. P., and G. E. Loeb. Mathematical models of proprioceptors: II. Structure and function of the Golgi tendon organ. *J. Neurophysiol.* 96(4):1172–1802, 2006.

[39]Murray, W. M., T. S. Buchanan, and S. L. Delp. The isometric functional capacity of muscles that cross the elbow. *J. Biomech.* 33:943–952, 2000.

[40]Murray, W. M., S. L. Delp, and T. S. Buchanan. Variation of muscle moment arms with elbow and forearm position. *J. Biomech.* 28:513–525, 1995.

[41]Perreault, E. J., R. F. Kirsch, and P. E. Crago. Voluntary control of static endpoint stiffness during force regulation tasks. *J. Neurophysiol.* 87:2808–2816, 2002.

[42]Schweighofer, N., M. A. Arbib, and M. Kawato. Role of the cerebellum in reaching movements in humans. I. Distributed inverse dynamics control. *Eur. J. Neurosci.* 10:86–94, 1998.

[43]Scott, S. H., and G. E. Loeb. The computation of position sense from spindles in mono- and multiarticular muscles. *J. Neurosci.* 14:7529–7540, 1994.

[44]Seireg, A., and R. Arvikar. Biomechanical Analysis of the Musculoskeletal Structure for Medicine and Sports. Hemisphere Publishing Corp., p. 93, 1989.

[45]Song, D., N. Lan, and J. Gordon. Biomechanical constraints on equilibrium point control of the multi-joint arm. A simulation study, ASB 2007 Conference, Stanford Univ., CA, August 2007.

[46]Song, D., M. Mileusnic, N. Lan, and J. Gordon. A sensorimotor systems model for dynamic simulation of arm movement control. In: 16th Annual Neural Control of Movement Meeting. Key biscayn Florida, USA: 2006.

[47]Stein, R. B., D. J. Weber, Y. Aoyagi, A. Prochazka, J. B. M. Wagenaar, S. Shoham, and R. A. Normann. Coding of position by simultaneously recorded sensory neurones in the cat dorsal root ganglion. *J. Physiol. Lond.* 560:883–896, 2004.

[48]Veeger, H. E. J, B. Yu, K. N. An, and R. H. Rozendal. Parameters for modeling the upper extremity. *J. Biomech.* 30:647–652, 1997.

[49]Wood, J. E., S. G. Meek, and S. C. Jacobsen. Quantitation of human shoulder anatomy for prosthetic arm control. 1. Surface modeling. *J. Biomech.* 22:273, 1989.

[50]Wu, G., F. C. T. van der Helm, H. E. J. Veeger, M. Makhsous, P. Van Roy, C. Anglin, J. Nagels, A. R. Karduna, K. McQuade, X. G. Wang, F. W. Werner, and B. Buchholz. ISB recommendation on definitions of joint coordinate systems of various joints for the reporting of human joint motion—Part II: shoulder, elbow, wrist and hand. *J. Biomech.* 38:981–992, 2005.

[51]Yakovenko, S., V. Gritsenko, and A. Prochazka. Contribution of stretch reflexes to locomotor control: a modeling study. *Biol. Cybern.* 90:146–155, 2004.

[52]Zajac, F. E. Muscle and tendon—properties, models, scaling, and application to biomechanics and motor control. *Crit. Rev. Biomed. Eng.* 17:359–411, 1989.